The landscape of circulating platelet aggregates in COVID-19

Keisuke Goda (goda@chem.s.u-tokyo.ac.jp)
University of Tokyo https://orcid.org/0000-0001-6302-6038

Yuqi Zhou
University of Tokyo

Masako Nishikawa
University of Tokyo

Hiroshi Kanno
University of Tokyo

Ting-Hui Xiao
University of Tokyo https://orcid.org/0000-0002-7339-152X

Takuma Suzuki
University of Tokyo

Shigekazu Takizawa
University of Tokyo

Jeffrey Harmon
University of Tokyo

Yuma Ibayashi
University of Tokyo

Kotaro Hiramatsu
University of Tokyo https://orcid.org/0000-0003-0767-019X

Nao Nitta
University of Tokyo https://orcid.org/0000-0002-9093-9016

Risako Kameyama
University of Tokyo

Walker Peterson
University of Tokyo

Jun Takiguchi
University of Tokyo

Mohammad Shifat-E-Rabbi
University of Virginia

Yan Zhuang
University of Virginia

Xuwang Yin

University of Virginia
Abu Rubaiyat
University of Virginia
Yunjie Deng
University of Tokyo
Hongqian Zhang
University of Tokyo
Gustavo Rohde
University of Virginia
Wataru Iwasaki
The University of Tokyo https://orcid.org/0000-0002-9169-9245
Yutaka Yatomi
University of Tokyo

Article

Keywords: Thrombotic Events, D-dimer Testing, Widespread Microthrombi, Large-scale Single-cell Image-based Profiling, Systemic Thrombosis

Posted Date: May 3rd, 2021

DOI: https://doi.org/10.21203/rs.3.rs-439419/v1

Abstract

A characteristic clinical feature of COVID-19 is the frequent occurrence of thrombotic events. Furthermore, many cases of multiorgan failure are thrombotic in nature. Since the outbreak of COVID-19, D-dimer testing has been used extensively to evaluate COVID-19-associated thrombosis, but does not provide a complete view of the disease because it probes blood coagulation, but not platelet activity. Due to this limitation, D-dimer testing fails to account for thrombotic events which occur despite low D-dimer levels, such as sudden stroke in young patients and autopsy-identified widespread microthrombi in multiple organs. Here we report the landscape of circulating platelet aggregates in COVID-19 obtained by large-scale single-cell image-based profiling and temporal monitoring of the blood of COVID-19 patients (n = 110). Surprisingly, our analysis shows the anomalous presence of excessive platelet aggregates in nearly 90% of all COVID-19 patients, including those who were not clinically diagnosed with thrombosis and those with low D-dimer levels (≤1 μg/mL). Additionally, results indicate a strong link between the concentration of platelet aggregates and the severity and mortality of COVID-19. Finally, high-dimensional analysis and comparison with other diseases reveal that COVID-19 behaves as a product of thrombosis (localized) and infectious diseases (systemic), as a cause of systemic thrombosis.

Main Text

With the increasing number of global case reports since the beginning of the COVID-19 pandemic, it has become clear that thrombosis is one of the primary factors for the severity and mortality of COVID-19[1-6]. In fact, an elevated level of D-dimers (>1 μg/mL) at admission has been associated with increased risk of requiring mechanical ventilation and death due to complications[9-12]. Thrombosis in COVID-19 is characterized by the frequent and simultaneous incidence of various types of thrombotic events in both arteries and veins[5], such as deep vein thrombosis (DVT), pulmonary embolism (PE), stroke, and myocardial infarction[1-6]. Patients with poor prognosis have been reported to be generally predisposed to thrombosis[4]. This is aligned with earlier autopsy reports on patients who died with COVID-19, which indicate widespread thrombotic microangiopathy characterized by extensive diffuse microthrombi present within small peripheral vessels in the lungs[17] and other organs[18,19]. In response to multiple reports that anticoagulant therapy with heparin leads to better prognosis in severe COVID-19 patients[21], both domestic and international organizations have issued clinical practice guidelines recommending that all hospitalized COVID-19 patients should receive thromboprophylaxis, or full therapeutic-intensity anticoagulation if prothrombotic conditions are present[22].

Unfortunately, the underlying processes and risk factors for the incidence of thrombotic events in COVID-19 remain elusive, resulting in thrombotic complications even under optimal anticoagulant therapy[23,24]. The root of the problem lies in the limitations of conventional diagnostic methods. For example, the D-dimer test is commonly used to estimate the presence of thrombi by measuring the cross-linked fibrin monomers (called D-dimers) produced when thrombi are degraded by fibrinolysis[25]. However, the test's specificity to thrombosis is low (typically 40-60%), since the concentration of D-dimers in the blood can

easily be raised by other factors such as cancer, pregnancy, and advanced age[26-30]. Also, the D-dimer test is conventionally used with a cutoff level typically set at 0.5-1 μg/mL to rule out thrombosis (mainly venous thrombosis such as DVT and PE)[29], but not as a quantitative measure; a high D-dimer level does not indicate the severity of the thrombotic event. Additionally, the D-dimer test is insensitive to platelet activity, which is critical for the initiation of thrombus formation, and cannot account for cases of large-vessel stroke reported as a presenting feature of COVID-19 among young patients (<40 years of age) even with low D-dimer levels (≤1 μg/mL)[14]. This suggests a different mechanism than common thrombosis[4]. On the other hand, optical microscopy can accurately probe platelet activity and has visualized platelet hyperactivity in COVID-19 by identifying the presence of platelet aggregates including macrothrombocytes[31]. However, visual inspection under the optical microscope is too slow and labor-intensive to analyze platelet aggregates in a statistically meaningful manner.

To better comprehend thrombosis in COVID-19, we used intelligent platelet morphometry[32-34] to perform large-scale image-based profiling and temporal monitoring of statistically significant numbers of circulating platelets and platelet aggregates in the blood of patients hospitalized with COVID-19 (n = 110) at single-cell resolution (Figure 1a, Extended Data Table 1). Specifically, our intelligent platelet morphometry machine, composed of an optical frequency-division-multiplexed (FDM) microscope[35,36] on a hydrodynamic-focusing microfluidic chip, enabled high-throughput, blur-free, bright-field image acquisition of a large population (n = 25,000 in total) of single platelets and platelet aggregates (including platelet-leukocyte aggregates) in each blood sample (1 mL) (Figure 1a, Figure 1b, Extended Data Table 1, Extended Data Figure 1a, Extended Data Figure 1b, Extended Data Figure 2). Figure 1c shows a library of typical bright-field images (67 x 67 pixels/image) of single platelets and platelet aggregates flowing at a high speed of 1 m/s, acquired within a field of view of 53.6 μm x 53.6 μm with a spatial resolution of 0.8 μm. Image acquisition was performed at a frequency of 3-5 times per week per hospitalized patient to observe temporal changes in the population and size distribution of platelet aggregates under various conditions such as anticoagulant therapy, mechanical ventilation, and discharge from the hospital (Extended Data Table 2). The ability of intelligent platelet morphometry to directly image platelet aggregates on a large statistical scale in real time made it possible to not only resolve and differentiate them with higher accuracy than flow cytometry[37] (especially between single platelets and small platelet aggregates), but also provide big image data for which advanced computational tools (e.g., high-dimensional analysis and deep learning) are effective[34,38].

Shown in Figure 2a are size distribution histograms and typical images of single platelets and platelet aggregates identified in the blood of typical patients with COVID-19 (see the complete dataset from all 110 patients in Source Data 1). Negative control data were also obtained from healthy subjects under the same sample preparation and image acquisition conditions on the same day to mitigate potential bias in the image data that may have come from experimental variations (e.g., fluctuations in optical alignment, hydrodynamic focusing conditions, blood draw, and sample preparation) and are also shown in the figure as references. The COVID-19 patients were categorized into three groups: (1) the mild patient group: those requiring no oxygen therapy; (2) the moderate patient group: those requiring oxygen therapy without

mechanical ventilation for respiratory support, such as extracorporeal membrane oxygenation (ECMO); and (3) the severe patient group: those requiring mechanical ventilation for respiratory support. Interestingly, as shown in Figure 2b, excessive platelet aggregates were also present in the blood of patients with low D-dimer levels (≤1 μg/mL). Figure 2c shows temporal changes in the size distribution histograms of single platelets and platelet aggregates identified in the blood of typical severe COVID-19 patients under anticoagulant therapy, reflecting their pathological conditions (see the complete dataset in Source Data 1 and the measurement days in Extended Data Table 2). It is important to note that we identified several cases of excessive platelet aggregates relapsed even after discharge from the hospital after anticoagulant therapy with heparin, which agrees with previous reports on post-discharge thrombosis in COVID-19[39,40].

We performed a statistical analysis of the landscape of circulating platelet aggregates to visualize trends and correlations. Figure 3a compares the platelet aggregate concentrations of mild, moderate, and severe COVID-19 patients on the highest concentration day of each hospitalized patient. The concentration of platelet aggregates was defined as the number of platelet aggregates divided by the number of all single platelets and platelet aggregates identified in 25,000 acquired images. Negative control data (shown as “control” in Figure 3a through Figure 3g) were provided by blood samples from healthy subjects (n = 4) on 67 different dates. The figure shows the anomalous presence of excessive platelet aggregates in as many as 87.3% of all COVID-19 patients, including those who were not clinically diagnosed with thrombosis and those with D-dimer levels below the reference level of ≤1 μg/mL at the University of Tokyo Hospital (see “statistical analysis” in the Methods section for details). The excessive platelet aggregation identified in each individual sample is consistent with earlier reports of averaged platelet hyperactivity detected by platelet function tests and gene expression analysis[41,42]. The figure also indicates a strong link between the severity of patients and the concentration of platelet aggregates. Moreover, results show an increase in the concentrations of platelet aggregates between measurements taken on the first day after admission (Figure 3b) and on the highest concentration day (Figure 3a) (typically ~1 week after the first measurement day), in agreement with previous reports on COVID-19 patients who developed thrombosis ~1 week after their initial symptoms appeared[10,43]. Likewise, Figure 3c shows a strong correlation between the mortality of patients and the concentration of platelet aggregates. Finally, Figure 3d and Figure 3e show that the presence of leukocytes in platelet aggregates is linked with the levels of severity and mortality, respectively, which is also consistent with previous reports on leukocyte hyperactivity in COVID-19[10,44-46]. These results may suggest the development of strategies for hospitalization and therapy at an early stage, even for COVID-19 patients without clear symptoms.

Next, we analyzed patient cases with D-dimer levels below the reference level of ≤1 μg/mL, which constitute 39.1% of all COVID-19 patients (n = 110). As shown in Figure 3f, significant levels of platelet aggregate concentrations are evident. Also, similar to the relation shown in Figure 3a, the link between the severity of patients and the concentration of platelet aggregates also persists, regardless of the patients’ D-dimer levels (Figure 3g). The figure shows that excessive platelet aggregates were found in as many as

76.7% of patients with a D-dimer level of ≤1 μg/mL (see “statistical analysis” in the Methods section for details). These results indicate the presence of a non-negligible thrombotic risk that could not be detected by the D-dimer test. This can be understood by the weak relationship between the D-dimer level and the concentration of platelet aggregates, as indicated by Pearson’s correlation coefficient of 0.225 (Extended Data Figure 3). In other words, as stated above, the D-dimer test evaluates blood coagulation by measuring D-dimers after thrombus degradation, whereas intelligent platelet morphometry characterizes platelet activity by profiling the statistics of platelet aggregates both before thrombus formation and after thrombus degradation. The latter method is therefore sensitive with high resolution to platelet hyperactivity, which is a suggested mechanism of widespread microthrombus formation (difficult to detect with the D-dimer test)[41,47].

Finally, we compared the concentrations of platelet aggregates from patients with COVID-19 and patients with other diseases that are known to produce platelet aggregates (Figure 3h, Extended Data Table 3, Extended Data Figure 4). Interestingly, the average concentration of platelet aggregates in COVID-19 is higher than that in thrombosis (e.g., stroke, DVT, PE; n = 16) and is close to that in other infectious diseases (e.g., pneumonia, pyelonephritis, cholangitis; n = 7) which are known to cause cytokine-mediated coagulation activation and the formation of neutrophil extracellular traps, which is similar to the platelet activation process of COVID-19. The results can be understood by recognizing that COVID-19 is a systemic disease caused by persistent endothelial cell activation upon SARS-CoV-2’s infection of the vascular endothelium[48], resulting in platelet aggregation which may or may not involve D-dimer production[4, 49], whereas thrombosis is a localized disease in which the platelet aggregates produced at the site of thrombi are diluted in the circulation. Additionally, as shown in Figure 3i, our deep-learning-based high-dimensional comparison of the images of platelet aggregates in COVID-19 with those in thrombosis and other infectious diseases, using the same image data shown in Figure 3h, shows that while platelet aggregates in non-COVID-19 infectious diseases and non-COVID-19 thrombosis are clearly different, platelet aggregates in COVID-19 have properties of both disease types. Likewise, as shown in Figure 3j, our comparison of the images of platelet aggregates in COVID-19 without risk factors for thrombosis (i.e., without thrombosis-related underlying conditions) (n = 22) with those in non-COVID-19 with risk factors only for venous thrombosis (cancer, post-surgery, long-term bed rest, obesity, and heart failure; n = 18) and with risk factors only for arterial thrombosis (hypertension, diabetes, hyperlipidemia, smoking, and history of atherosclerosis; n = 15) indicates that while platelet aggregates in the two risk factor groups are distinct[50], platelet aggregates in COVID-19 have characteristics of both groups, with a stronger overlap with the venous thrombosis risk factor group, which is consistent with earlier reports on the diversity of COVID-19-associated thrombosis[3-5] as well as the statistics of its types as reported by international societies on thrombosis and hemostasis (arterial thrombosis: ~30%; venous thrombosis: ~70%). Although thrombosis and infectious diseases are known discretely as localized and systemic diseases, respectively, our results indicate that COVID-19 cannot be classified easily into either category; COVID-19 instead behaves as a product of the two disease classes, as a cause of systemic thrombosis.

Methods

Human subjects

The subjects used in this study were patients who were clinically diagnosed with COVID-19 based on their reverse transcription polymerase chain reaction (RT-PCR) test results (Extended Data Table 1). Blood samples were collected as residual coagulation test samples (with 3.2% citrate) after the completion of requested clinical laboratory tests for diagnosing COVID-19 at the University of Tokyo Hospital. The negative control group was composed of 4 healthy subjects. Blood samples from the healthy subjects were drawn multiple times on 67 different dates for preparing control samples. Likewise, the positive control group was composed of 7 hospitalized patients under no anticoagulant therapy and with no abnormality confirmed by their coagulation tests, which indicated PT-INR (prothrombin time and international normalized ratio), APTT (activated partial thromboplastin time), and fibrinogen levels of 0.88 - 1.10, 24 - 34 sec, and 168 - 355 mg/dL, respectively, and D-dimer levels of less than 1 μg/mL. Subjects under anticoagulant therapy were excluded. Clinical information and laboratory test data were obtained from the electronic medical records of the patients using a standardized data collection form. For comparison, blood samples from subjects with other diseases that elevate D-dimer levels, such as cancer, thrombosis, and sepsis were also analyzed. This study was conducted with the approval of the Institutional Ethics Committee in the School of Medicine at the University of Tokyo [no. 11049, no. 11344] in compliance with the relevant guidelines and regulations. Written informed consent for participation in the study was obtained from the patients using an opt-out process on the webpage of the University of Tokyo Hospital. Patients who refused participation in our study were excluded. Written informed consent was obtained from the healthy subjects as well. The demographics, clinical characteristics, and laboratory findings of patients with COVID-19 are shown in Extended Data Table 1. The demographics, clinical characteristics, and laboratory findings of patients with other diseases (e.g., cancer, non-COVID-19 thrombosis, non-COVID-19 infectious diseases) are shown in Extended Data Table 3.

Sample preparation

Single platelets and platelet aggregates were enriched from whole blood by density-gradient centrifugation to maximize the efficiency of detecting platelets and platelet aggregates, as described in our previous report[32] with minor modifications. As shown in Extended Data Figure 2, for analyzing the concentration of platelet aggregates, 500 μL of blood was diluted with 5 mL of saline. Platelets were isolated by using Lymphoprep (STEMCELLS, ST07851), a density-gradient medium, based on the protocol provided by the vendor. Specifically, the diluted blood was added to the Lymphoprep medium and centrifuged at 800 g for 20 min. After the centrifugation, 500 μL of the sample was taken from the mononuclear layer. Platelets were immunofluorescently labeled by adding 10 μL of anti-CD61-PE (Beckman Coulter, IM3605) and 5 μL of anti-CD45-PC7 (Beckman Coulter, IM3548) to the blood sample to ensure the detection of all platelets or platelet aggregates in the sample. Then, 500 μL of 2% paraformaldehyde (Wako, 163–20145) was added for fixation. The operation was performed at room temperature.

Laboratory tests

Blood samples from the patients were used for routine laboratory tests, such as leukocyte count, platelet count, alanine transaminase (ALT) concentration, creatinine concentration, lactate dehydrogenase concentration, C-reactive protein concentration, and D-dimer level (Extended Data Table 1). All the D-dimer tests were conducted on a CN6500 automatic coagulation analyzer (Sysmex, Japan) with a latex-enhanced photometric immunoassay (LIAS AUTO D-dimer NEO, Sysmex, Japan). The laboratory reference range of the D-dimer test at the University of Tokyo Hospital was 0 - 1.0 μg/mL.

Intelligent platelet morphometry machine

The intelligent platelet morphometry machine mainly consists of two parts: image acquisition and digital image analysis (Figure 1a, Extended Data Figure 1a). For image acquisition, the FDM microscope was used for acquiring high-speed, blur-free, bright-field images of flowing cells (e.g., red blood cells, leukocytes, platelets, platelet aggregates, cell debris) with 67 x 67 pixels per image at a high throughput of 100 - 250 events per sec (eps), where an event is defined as a single platelet or a platelet aggregate since red blood cells, leukocytes, and cell debris were not detected as events. The throughput was chosen to avoid clogging the microchannel although the theoretical throughout of the machine was >10,000 eps. The FDM microscope used a broadband, spatially distributed, optical frequency comb to illuminate flowing cells in a microfluidic channel. The image-encoded time-domain signal was detected with a single-pixel photodetector, converted into a serial digital data stream by a digitizer, and recovered as bright-field images by a home-made LabVIEW program. For each blood sample, objective areas in 25,000 acquired images were plotted in a size distribution histogram.

Optical frequency-division-multiplexed microscope

The FDM microscope is a high-speed, blur-free, bright-field imaging system based on a spatially distributed optical frequency comb as the optical source and a single-pixel photodetector as the image sensor[35, 36]. Since the optical frequency comb is composed of multiple beams which are spatially distributed, it is capable of simultaneously interrogating the one-dimensional spatial profile of a target object (e.g., a platelet, a platelet aggregate). In addition, since each discrete beam of the optical frequency comb is tagged by a different modulation frequency, a spatial-profile-encoded image can be retrieved by performing Fourier transformation on the time-domain waveform detected by the single-pixel detector. As shown in Extended Data Figure 1b, we used a continuous-wave laser (Cobolt Calypso, 491 nm, 100 mW) as the laser source. Emitted light from the laser was split by a beam splitter, deflected and frequency-shifted by acousto-optic deflectors (Brimrose TED-150-100-488, 100-MHz bandwidth), and recombined by another beam splitter. The resultant optical frequency comb was focused by an objective lens (Olympus UPLSAPO20X, NA:0.75) onto objects (e.g., single platelets, platelet aggregates) flowing at 1 m/s in a customized hydrodynamic-focusing microfluidic channel (Hamamatsu Photonics). Light transmitted through the flowing objects was collected by an avalanche photodiode (Thorlabs APD430A/M) and processed by a home-made LabVIEW program to reconstruct the bright-field images. The line scan rate, spatial resolution, field of view, and number of pixels were 3 MHz, 0.8 μm, 53.6 μm x 53.6 μm, and 67 x 67 pixels, respectively. Fluorescence emitted from platelets labeled by anti-CD61-PE was also collected and

used for triggering image acquisitions. Fluorescence emitted from leukocytes labeled by anti-CD45-PC7 was collected to identify platelet aggregates containing leukocytes.

Statistical analysis

The regions of objects (i.e., platelets, platelet aggregates) in bright-field images were segmented in MATLAB for calculating the concentration of platelet aggregates in each sample. First, a 10x interpolation by the interp2 function (MATLAB) was applied to each image for achieving segmentation results. Then, the outlines of the object regions were detected by using the edge detection function with the Canny method in MATLAB. Morphological operations like dilate, fill, and erode were applied to fill and refine the object regions for obtaining their masks as well as for eliminating the background noise. After the segmentation, the size of the object (i.e., a single platelet, a platelet aggregate) in each image was calculated by multiplying the pixel size of the segmented region, which was extracted by the regionprops function, and the pixel resolution (80 nm/pixel) after interpolation. All the images with objective areas larger than 48 μm^2 were considered as the images of platelet aggregates in all the patient and healthy subject (control) samples. The concentration of platelet aggregates was defined by the ratio of the number of acquired images containing platelet aggregates to the total number of acquired images containing single platelets and platelet aggregates (n = 25,000) in each sample. In all 110 patient datasets, 106 of them have 25,000 images while only 4 of them (no. 6, 10, 12, 14) have 20,000 images due to a data-recording error, but this should not influence the statistical accuracy of our data analysis since the number of acquired images is significantly large. The presence of leukocytes in platelet aggregates was also identified by analyzing the morphology of the platelet aggregates by their images. For confirmation, the fluorescence signal of anti-CD61-PE and anti-CD45-PC7 was also used. CD61-PE/CD45-PC7 double-positive events were counted as platelet aggregates containing leukocytes. CD61-PE positive and CD45-PC7 negative events that had CD61-PE signal intensity greater than a threshold value were counted as platelet aggregates excluding leukocytes. The presence of excessive platelet aggregates was determined by calculating the mean and standard deviation of the distribution of the concentration of platelet aggregates in the control samples and evaluating if the concentration of platelet aggregates in a patient sample exceeded the threshold (mean + standard deviation). If a tighter threshold (mean + two standard deviations) was used to calculate the presence of excessive platelet aggregates, then the ratio of the number of patients with excessive platelet aggregates to the number of all patients is 75.5%, while the ratio of the number of patients with excessive platelet aggregates and low D-dimer levels (≤1 μg/mL) to the number of all patients with low D-dimer levels (≤1 μg/mL) is 62.8%.

High-dimensional analysis

In both Figure 3i and Figure 3j, a fully connected classifier was trained on image data from non-COVID-19 patient blood samples under specific classes to build a visual feature extractor. The class label was represented as a one-hot vector. Images were picked with size gating and normalized to zero mean and unit variance. The images were input into VGG-16 with pre-trained weights on ImageNet dataset. The output of the fourth pooling layer was flattened into an 8192-dimensional vector and input into the

classifier. The classifier was optimized by Adam optimizer with loss function of mean absolute error. To improve classification accuracy for under-represented classes, the loss function was weighted by inverse class frequency. The learning rate was reduced from 0.01 by a factor of 0.31 when the validation loss stopped decreasing for more than 10 epochs. The training was terminated when there was no significant improvement for 100 epochs. The training and validation set was randomly selected with an 80/20 ratio. After the training, the final layer was removed and the rest was used as a feature extractor, which output a 48-dimensional vector. The dimension of feature vectors was reduced into minimum dimension by principal component analysis, so that cumulative contribution rate of the selected principal components was more than 0.99. For Figure 3i, 13770 images of platelet aggregates from 16 thrombosis patients and 12651 images of platelet aggregates from 7 infectious disease patients were used for the training and validation and displayed in the uniform manifold approximation and projection (UMAP) plot. 150116 images of platelet aggregates from 110 COVID-19 patients were added to the UMAP plot. The feature extractor was implemented in Tensorflow. VGG-16 was used as the application in the library. Figure 3i was plotted with parameters n_neighbor = 1000 and min_dist = 1. For Figure 3j, 19649 images of platelet aggregates from 15 patients with risk factors for venous thrombosis (hypertension, diabetes, hyperlipidemia, smoking, and history of atherosclerosis) 20850 images of platelet aggregates from 18 patients with risk factors for arterial thrombosis (cancer, post-surgery, long-term bed rest, obesity, and heart failure) were used for the training and validation and displayed in the UMAP plot. Patients in each group did not have risk factors for the diseases in the other groups. To show their relations with the diseases, 22890 images of platelet aggregates from 22 COVID-19 patients without thrombosis-related underlying conditions were added to the UMAP plot. Figure 3j was plotted with n_neighbor = 4000 and min_dist = 1.

Data availability

The source data (Source Data 1) supporting the findings of this study are available at http://doi.org/10.5281/zenodo.4700112 and are also available from the corresponding authors upon reasonable request.

Code availability

All the code used for data taking and analysis in this study is available at http://doi.org/10.5281/zenodo.4700072 and is also available from the corresponding authors upon reasonable request.

Declarations

Acknowledgements

This work was supported by AMED JP20wm0325021, JSPS Core-to-Core Program, JSPS KAKENHI grant numbers 19H05633 and 20H00317, ImPACT Program (CSTI, Cabinet Office, Government of Japan), White Rock Foundation, Ogasawara Foundation, Nakatani Foundation, Konica Minolta Foundation, and

Charitable Trust Laboratory Medicine Research Foundation of Japan. We thank Kyoko Hasegawa and Yoshika Kusumoto for help with the sample preparation.

Author information

Contributions

K. G. conceived the work. H. K., Y. Z., T. X., and K. G. designed the intelligent platelet morphometry machine. H. K. built the machine. M. N., J. T., and Y. Z. prepared the blood samples. H. K., Y. I., and M. N. performed the image acquisition of platelets and platelet aggregates. Y. Z., S. T., M. R., T. S., and G. R. analyzed the image data. J. H., S. T., Y. D., H. Z., K. H., R. K., W. P., M. S., Y. Z. X. Y., A. R., G. R., and W. I. helped the image data acquisition and analysis. Y. Z., M. N., T. X., N. N., Y. Y., and K. G. interpreted the analysis results. T. X., Y. Y., and K. G. supervised the work. All others participated in writing the paper.

Corresponding authors

Correspondence to Keisuke Goda (goda@chem.s.u-tokyo.ac.jp), Ting-Hui Xiao (xiaoth@chem.s.u-tokyo.ac.jp), Yutaka Yatomi (yatoyuta-tky@umin.ac.jp)

Ethics declarations

N. N. and K. G. are shareholders of CYBO, Inc. The other authors have no competing interests.

References

1. Zhou, F. et al. Clinical course and risk factors for mortality of adult inpatients with COVID-19 in Wuhan, China: a retrospective cohort study. *Lancet* **395,** 1038-1038 (2020).
2. Ali, M. A. M. et al. COVID-19 and thrombosis: from bench to bedside. *Trends Cardiovas. Med.* **31,** 143-160 (2021).
3. Willyard, C. Coronavirus blood-clot mystery intensifies. *Nature* **581,** 250-250 (2020).
4. Merrill, J. T. et al. Emerging evidence of a COVID-19 thrombotic syndrome has treatment implications. *Rev. Rheumatol.* **16,** 581-589 (2020).
5. Fraisse, M. et al. Thrombotic and hemorrhagic events in critically ill COVID-19 patients: a French monocenter retrospective study. *Care.* **24,** 275 (2020).
6. Katneni, U. K. et al. Coagulopathy and thrombosis as a result of severe COVID-19 infection: a microvascular focus. *Haemostasis* **120,** 1668-1679 (2020).
7. Guan, W. et al. Clinical characteristics of coronavirus disease 2019 in China. *New Engl. J. Med.* **382,** 1708-1720 (2020).
8. Gupta, A. et al. Extrapulmonary manifestations of COVID-19. *Med.* **26,** 1017-1032 (2020).
9. Yu, H. H. et al. D-dimer level is associated with the severity of COVID-19. *Res.* **195,** 219-225 (2020).

10. Arachchillage, D. R. J. et al. Abnormal coagulation parameters are associated with poor prognosis in patients with novel coronavirus pneumonia. *Thromb. Haemost.* **18,** 1233-1234 (2020).
11. Zhang, L. T. et al. D-dimer levels on admission to predict in-hospital mortality in patients with Covid-19. *Thromb. Haemost.* **18,** 1324-1329 (2020).
12. Yao, Y. M. et al. D-dimer as a biomarker for disease severity and mortality in COVID-19 patients: a case control study. *Intensive. Care.* **8,** 49 (2020).
13. Adam, S. S. et al. D-dimer antigen: current concepts and future prospects. *Blood* **113,** 2878-2887 (2009).
14. Oxley, T. J. et al. Large-vessel stroke as a presenting feature of COVID-19 in the young. *Engl. J. Med.* **382,** e60 (2020).
15. Fifi, J. T. et al. COVID-19 related stroke in young individuals. *Lancet Neurol.* **19,** 713-715 (2020).
16. Ellul, M. A. et al. Neurological associations of COVID-19. *Lancet Neurol.* **19,** 767-783 (2020).
17. Ackermann, M. et al. Pulmonary vascular endothelialitis, thrombosis, and angiogenesis in COVID-19. *New Engl. J. Med.* **383,** 120-128 (2020).
18. Bois, M. C. et al. COVID-19-associated nonocclusive fibrin microthrombi in the heart. *Circulation* **143,** 230-243 (2021).
19. Pellegrini, D. et al. Microthrombi as a major cause of cardiac injury in COVID-19: a pathologic study. *Circulation* **143,** 1031-1042 (2021).
20. Bradley, B. T. et al. Histopathology and ultrastructural findings of fatal COVID-19 infections in Washington State: a case series. *Lancet* **396,** 312-312 (2020).
21. Tang, N. et al. Anticoagulant treatment is associated with decreased mortality in severe coronavirus disease 2019 patients with coagulopathy. *Thromb. Haemost.* **18,** 1094-1099 (2020).
22. Thachil, J. et al. ISTH interim guidance on recognition and management of coagulopathy in COVID-19. *Thromb. Haemost.* **18,** 1023-1026 (2020).
23. Lodigiani, C. et al. Venous and arterial thromboembolic complications in COVID-19 patients admitted to an academic hospital in Milan, Italy. *Res.* **191,** 9-14 (2020).
24. Paranjpe, I. et al. Association of treatment dose anticoagulation with in-hospital survival among hospitalized patients with COVID-19. *Am. Coll. Cardiol.* **76,** 122-124 (2020).
25. Wells, P. S. et al. Evaluation of D-dimer in the diagnosis of suspected deep-vein thrombosis. *New Engl. J. Med.* **349,** 1227-1235 (2003).
26. Urban, K. et al. It's time to use an age-based approach to D-dimer. *Fam. Practice* **63,** 155-158 (2014).
27. Schrecengost, J. E. et al. Comparison of diagnostic accuracies in outpatients and hospitalized patients of D-Dimer testing for the evaluation of suspected pulmonary embolism. *Chem.* **49,** 1483-1490 (2003).
28. Raja, A. S. et al. Evaluation of patients with suspected acute pulmonary embolism: best practice advice from the clinical guidelines committee of the american college of physicians. *Intern. Med.* **163,** 701-711 (2015).

29. Kabrhel, C. et al. Factors associated with positive D-dimer results in patients evaluated for pulmonary embolism. *Emerg. Med.* **17**, 589-597 (2010).
30. Sartori, M. et al. The wells rule and D-dimer for the diagnosis of isolated distal deep vein thrombosis. *Thromb. Haemost.* **10,** 2264-2269 (2012).
31. Rampotas, A. et al. Platelet aggregates, a marker of severe COVID-19 disease. *Clin. Pathol.* **0,** 1-2 (2020).
32. Zhou, Y. Q. et al. Intelligent classification of platelet aggregates by agonist type. *Elife* **9,** e52938 (2020).
33. Nitta, N. et al. Intelligent image-activated cell sorting. *Cell* **175,** 266-276 (2018).
34. Zhou, Y. et al. Intelligent platelet morphometry. *Trends Biotechnol.* https://doi.org/10.1016/j.tibtech.2020.12.012 (2021).
35. Mikami, H. et al. Ultrafast confocal fluorescence microscopy beyond the fluorescence lifetime limit. *Optica* **5,** 117-126 (2018).
36. Kanno, H. et al. Simple, stable, compact implementation of frequency-division-multiplexed microscopy by inline interferometry. *Lett.* **44,** 467-470 (2019).
37. Cossarizza, A. et al. Guidelines for the use of flow cytometry and cell sorting in immunological studies (second edition). *J. Immunol.* **49**, 1457-1973 (2019).
38. Isozaki, A. et al. AI on a chip. *Lab Chip* **20**, 3074-3090 (2020).
39. Patell, R. et al. Postdischarge thrombosis and hemorrhage in patients with COVID-19. *Blood* **136,** 1342-1346 (2020).
40. Salisbury, R. et al. Incidence of symptomatic, image-confirmed venous thromboembolism following hospitalization for COVID-19 with 90-day follow-up. *Blood Adv.* **4,** 6230-6239 (2020).
41. Comer, S. P. et al. COVID-19 induces a hyperactive phenotype in circulating platelets. *PLOS Biol.* **19,** e3001109 (2021).
42. Manne, B. K. et al. Platelet gene expression and function in patients with COVID-19. *Blood* **136,** 1317-1329 (2020).
43. Middeldorp, S. et al. Incidence of venous thromboembolism in hospitalized patients with COVID-19. *Thromb. Haemost.* **18,** 1995-2002 (2020).
44. Hottz, E. D. et al. Platelet activation and platelet-monocyte aggregate formation trigger tissue factor expression in patients with severe COVID-19. *Blood* **136,** 1330-1341 (2020).
45. Zuo, Y. et al. Prothrombotic autoantibodies in serum from patients hospitalized with COVID-19. *Transl. Med.* **12,** eabd3876 (2020).
46. Le Joncour, A. et al. Neutrophil-platelet and monocyte-platelet aggregates in COVID-19 patients. *Haemostasis* **120**, 1733-1735 (2020).
47. Zhang, S. et al. SARS-CoV-2 binds platelet ACE2 to enhance thrombosis in COVID-19. *Hematol. Oncol.* **13,** 120 (2020).

48. Ward, S. E. et al. Von Willebrand factor propeptide in severe coronavirus disease 2019 (COVID-19): evidence of acute and sustained endothelial cell activation. *J. Haematol.* **192,** 714-719 (2021).
49. Levi, M. et al. Coagulation abnormalities and thrombosis in patients with COVID-19. *Lancet Haematol.* **7,** E438-E440 (2020).
50. Mackman, N. New insights into the mechanisms of venous thrombosis. *Clin. Invest.* **122,** 2331-2336 (2012).

Figures

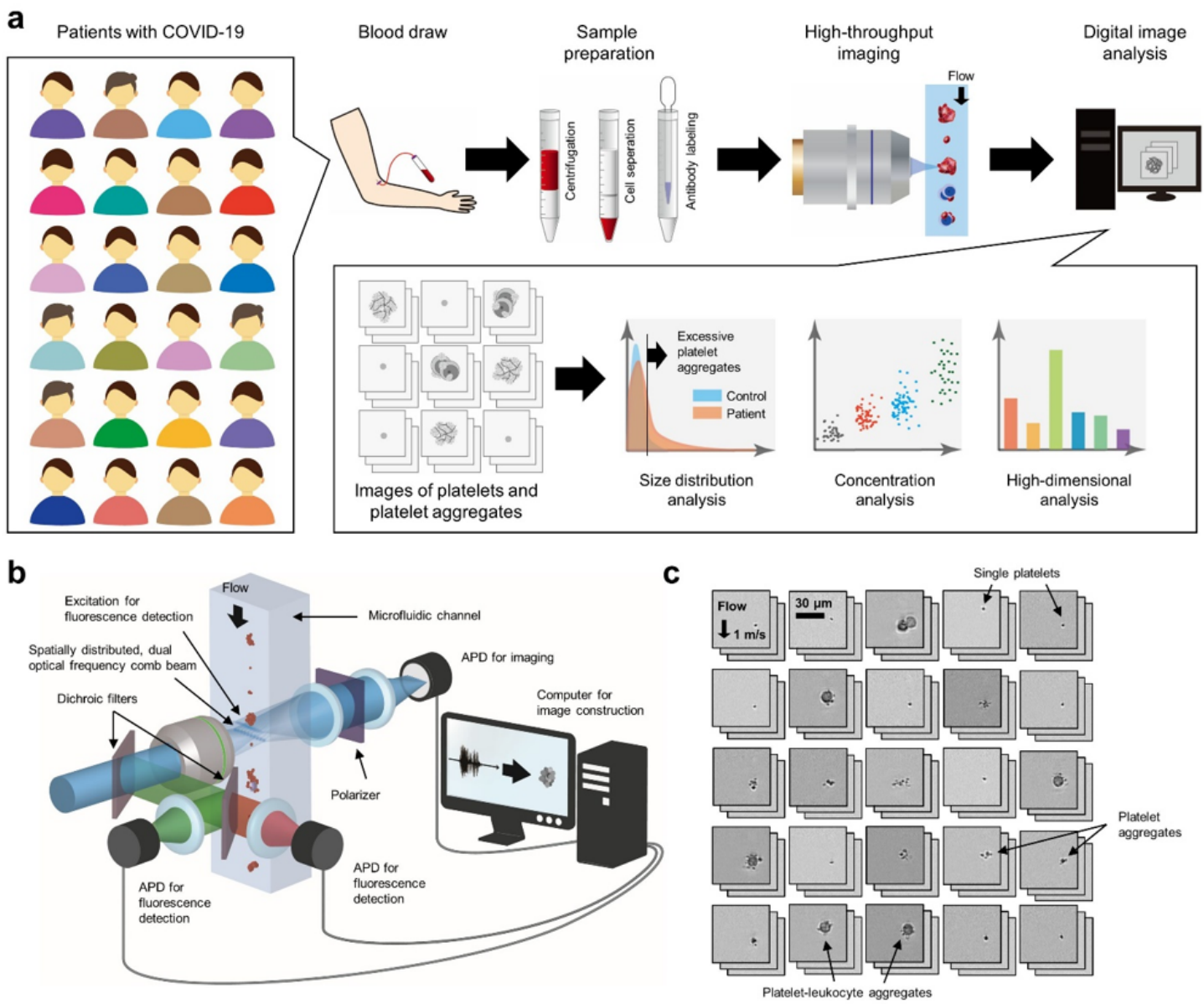

Figure 1

Intelligent platelet morphometry for large-scale image-based profiling of circulating platelet aggregates at single-cell resolution. a, Experimental workflow consisting of blood draw, sample preparation, high-

throughput imaging, and digital image analysis. b, Schematic of the optical frequency-division multiplexed microscope in the intelligent platelet morphometry machine. APD: avalanche photodetector. c, Typical bright-field images of single platelets and platelet aggregates obtained by the intelligent platelet morphometry machine.

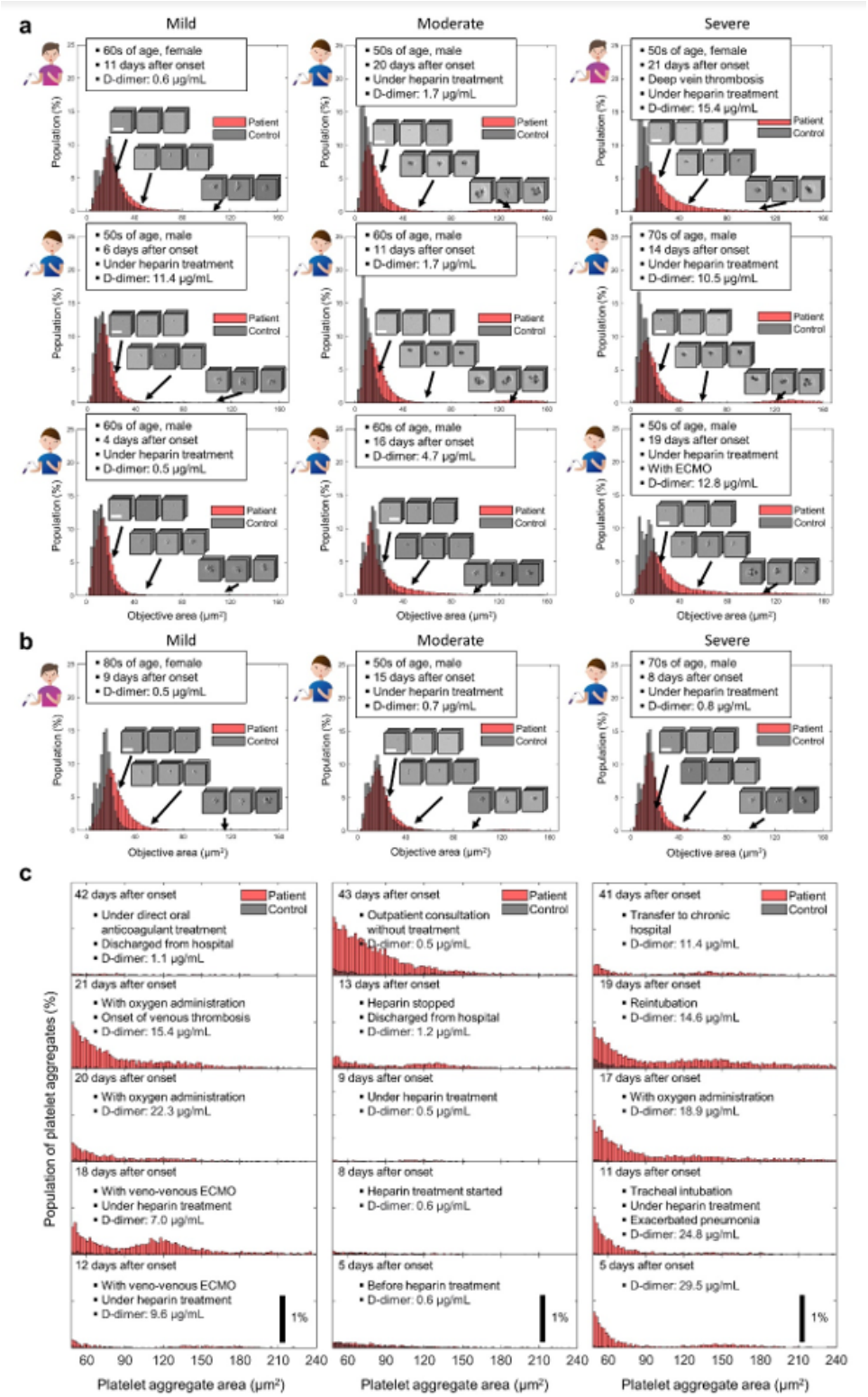

Figure 2

Statistics of platelet aggregates in the blood of patients with COVID-19. a, Size distribution histograms and typical images of single platelets and platelet aggregates in the blood of mild, moderate, and severe patients with COVID-19. The clinical information and D-dimer level of each patient are also shown in the insets. b, Size distribution histograms and typical images of single platelets and platelet aggregates in the blood of typical mild, moderate, and severe patients with COVID-19 and low D-dimer levels (≤1 μg/mL). c, Temporal changes in the size distribution histograms of single platelets and platelet aggregates in the blood of severe patients with COVID-19 under anticoagulant therapy.

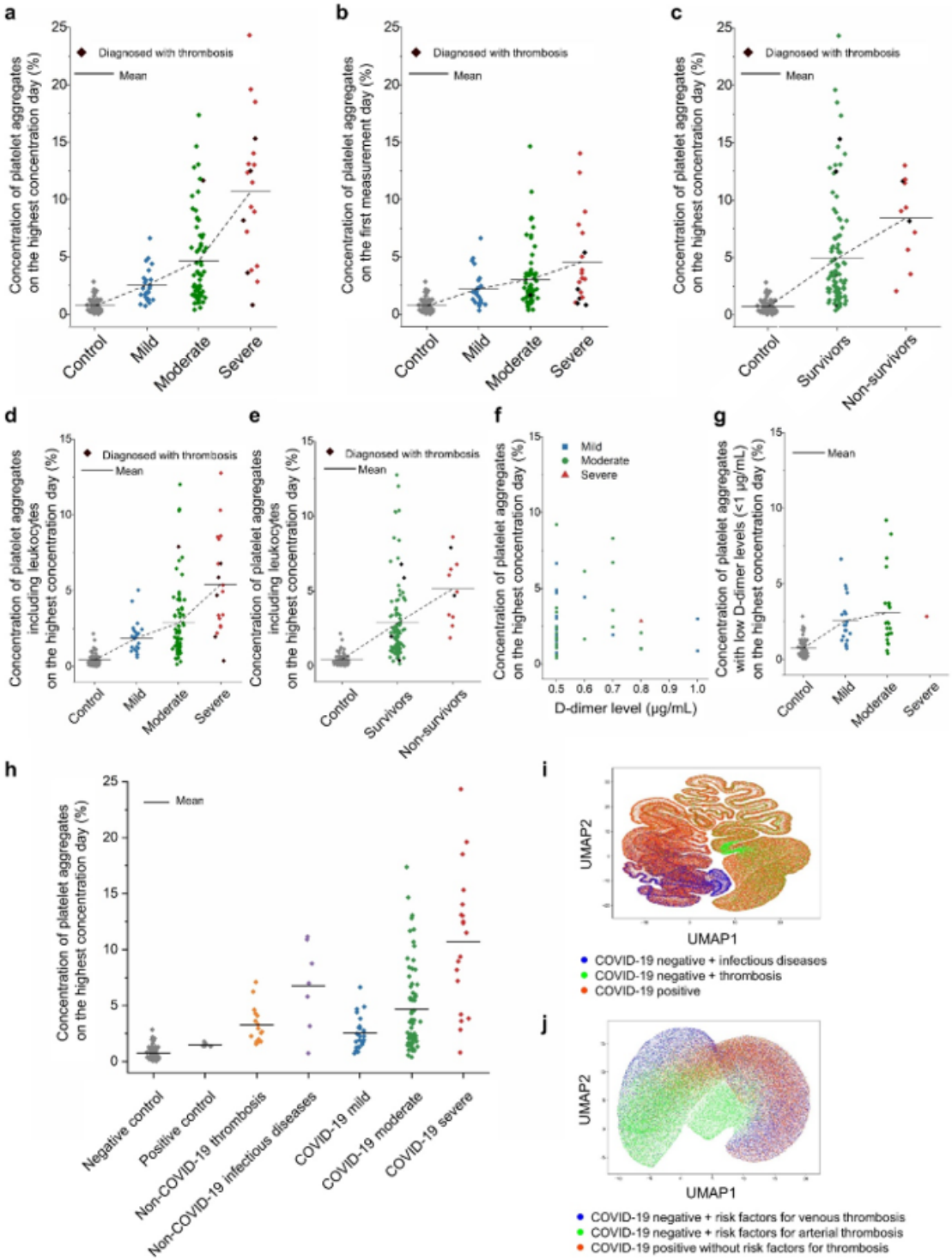

Figure 3

Statistical analysis of the platelet aggregate images. a, Comparison of the platelet aggregate concentrations of mild (n = 23), moderate (n = 68), and severe (n = 19) patients with COVID-19, measured on the highest concentration day of each hospitalized patient. For the definition of images containing platelet aggregates, see “statistical analysis” in the Methods section for details. b, Comparison of the platelet aggregate concentrations of mild (n = 23), moderate (n = 68), and severe (n = 19) patients with COVID-19 on the first measurement day of each hospitalized patient. c, Comparison of the platelet aggregate concentrations of survivors (n = 99) and non-survivors (n = 11) from COVID-19, measured on the highest concentration day of each hospitalized patient. d, Comparison of the concentrations of platelet aggregates of mild (n = 23), moderate (n = 68), and severe (n = 19) patients with COVID-19 including leukocytes, measured on the highest concentration day of each hospitalized patient. e, Comparison of the concentrations of platelet aggregates of survivors (n = 99) and non-survivors (n = 11) from COVID-19, measured on the highest concentration day of each hospitalized patient. f, Concentrations of platelet aggregates of patients with COVID-19 (39.1% of n = 110) and low D-dimer levels (≤1 μg/mL). g, Comparison of the platelet aggregate concentrations of mild (n = 17), moderate (n = 22), and severe (n = 1) patients with COVID-19 and low D-dimer levels (≤1 μg/mL), measured on the highest concentration day of each hospitalized patient. h, Concentrations of platelet aggregates of patients with COVID-19 compared with those of the positive control group and patients with non-COVID-19 thrombosis (n = 16) and non-COVID-19 infectious diseases (n = 7). Negative control: healthy subjects; positive control: patients with diseases that do not produce platelet aggregates; thrombosis: patients with stroke, DVT, PE, etc. Non-COVID-19 infectious diseases below the disseminated intravascular coagulation (DIC) diagnostic criteria: patients with pneumonia, pyelonephritis, cholangitis, etc. i, UMAP plot of platelet aggregates from COVID-19 patients, non-COVID-19 infectious diseases, and non-COVID-19 thrombosis, using the same data shown in Figure 3h. j, UMAP plot of platelet aggregates from COVID-19 patients without risk factors for thrombosis (n = 22), non-COVID-19 patients with risk factors for venous thrombosis (n = 18), and non-COVID-19 patients with risk factors for arterial thrombosis (n = 15).

Supplementary Files

This is a list of supplementary files associated with this preprint. Click to download.

- extendeddatatable1v04.xlsx
- extendeddatatable2v02.xlsx
- extendeddatatable3v03.xlsx
- ExtendedData.docx